Supporting information to "Upward transport and segregation of ice-nucleating particles in deep convective clouds"

Jonas Schaefer[a], Sarah Grawe[a], Hans-Christian Clemen[b], Stephan Mertes[a], Johannes Schneider[b], Bruno Wetzel[a], Daniel Sauer[c], Jennifer Wolf[c], Laura Tomsche[c,d], Johanna Mayer[c], Roland Schrödner[a], Silvia Henning[a], Tina Jurkat-Witschas[c], Christiane Voigt[c,d], Helmut Ziereis[c], Theresa Harlaß[c], Mira Pöhlker[a,e], and Frank Stratmann[a]

[a]Leibniz Institute for Tropospheric Research TROPOS, Leipzig, Germany
[b]Max Planck Institute for Chemistry, Mainz, Germany
[c]Deutsches Zentrum für Luft- und Raumfahrt (DLR), Oberpfaffenhofen, Germany
[d]Johannes Gutenberg-Universität Mainz, Mainz, Germany
[e]Leipziger Institut für Meteorologie (LIM), Universität Leipzig, Leipzig, Germany

Correspondence: Jonas Schaefer (jschaefer@tropos.de)

1 INP measurements and processing

1.1 Calculation of INP concentrations

The number of optically recorded frozen droplets (LINA) / wells (INDA), ΔN, is used to calculate differential INP spectra for each filter sample (Vali, 1971) according to equations Eq. S1, with $k(T)$ being the number of additionally available INP for a finite decrease in temperature ΔT, and V is the sampled air volume normalization term calculated from the volumes of sampled air, washing water, and droplet (Eq. S2).

$$k(T) = -\frac{1}{V \times \Delta T} \ln(1 - \frac{\Delta N}{N(T)}) \tag{S1}$$

$$V = \frac{V_{\text{flow}}}{V_{\text{water}}} \cdot V_{\text{droplet/well}} \tag{S2}$$

The temperature interval for which the differential is calculated needs to be optimized (Vali, 2019) balancing temperature resolution of the INP spectra, and potential uncertainties due to bad counting statistics. Thereby, small ΔT imply a high temperature resolution, however the spectra may suffer from decreased accuracy because of poor counting statistics, as narrow temperature intervals imply a smaller number of droplets freezing. Consideration of larger ΔT usually results in a larger

number of freezing droplets, and consequently better counting statistics, however implies a lower temperature resolution. For the quantification of the UTLS background INP concentration, because of the low INP concentrations prevailing, a temperature interval of ΔT = 2 K was chosen. For the samples in and around deep convection, which feature compared to the UTLS background significantly higher INP concentrations, the temperature interval was set to ΔT = 1 K.

Integrating $k(T)$ over freezing temperature yields the commonly shown cumulative N_{INP}-temperature spectra.

1.2 Interference background

An important source of uncertainty when using freezing array type instruments for the determination of INP freezing spectra, is the method-inherent interference background, which results from droplet freezing induced by the freezing array instrument surface area, washing water impurities, and/or contamination caused by the filter handling procedure. In the framework of the present investigations, the interference background is determined from 19 blank filter samples taken throughout the campaign with at least one blank sample obtained during each flight. The blank filters were processed identical to the sample filters but without being subjected to an aerosol flow.

1.3 Monte-Carlo simulations

To account for uncertainties caused by counting statistics (Poisson statistics), Monte-Carlo (MC) simulations were performed for all filter samples and blank filters (Vali, 2019).

Thereto, the calculation of k was repeated using random sampled numbers from a Poisson distribution around the measured value of $dN(T)$ using the random.poisson function of the numpy python package (Harris et al., 2020). The number of MC simulations was set to N_{MC} = 10000.

An example of MC generated probability density function (PDF) of INP concentrations N_{INP} (active at -25 °C) is shown by the blue curve in Fig. S1a and the full INP-temperature spectra in Fig. S1b.

The blank filters are also processed using MC-simulations which yield 190 000 INP spectra representing the interference background, also shown in Fig.S1 by the red curves/boxes. With this, counting statistics are also accounted in addition to partly systematic variability of the interference background. The latter are presumably caused by minimal contamination of a small number of blanks in the field or during laboratory analysis hence the interference background PDF's are not log-normal at every temperature interval.

This specific sample, Filter 3 of research flight F10/11, was chosen to illustrate that the lower end of the sample's PDF may overlap with the PDF of the interference background.

1.4 Interference background subtraction

To account for potential effects of the interference background on the INP concentrations determined in course of the present investigations, a background subtraction (Vali, 2019) was carried out. For this, from each temperature-spectra generated by a MC Simulation for a particular sample, a randomly selected MC generated temperature spectra of the interference background

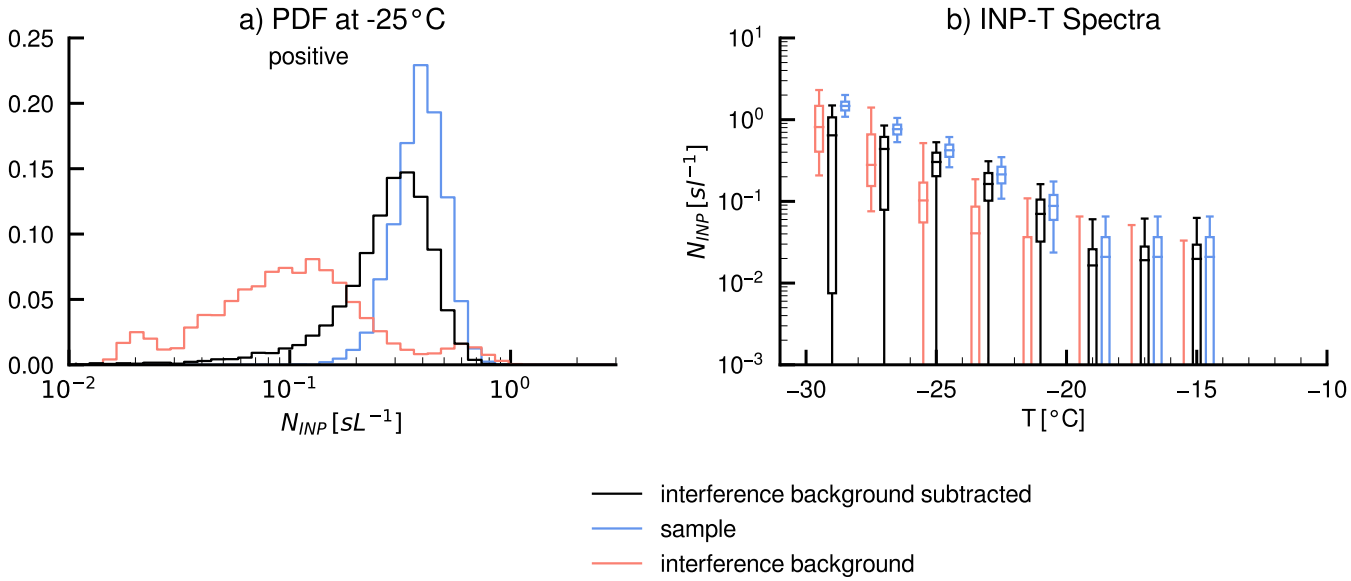

Figure S1. a) shows probability density function (PDF) of INP concentration at -25 °C effective temperature using LINA. The red curve indicates the interference background PDF of, the blue curve the PDF of the sample (F10/11 Filter 3, stratospheric sample) and the black curves shows the PDF of the sample after subtraction of the interference background. b) shows INP concentration-temperature spectra for the same sample. The box indicates the inter-quartile range, the central line in the box shows the median and the whiskers mark the 5th and 95th percentiles

was substracted. For each individual sample, this again yields a PDF (shown in Fig. S1, black line), which accounts for the variability of the interference background, and the Poisson uncertainties of both, the sample and blanks. If the sample exceeds the interference background only marginally (e.g. as shown in Fig. S1) the propagated Poisson error of the difference spreads over several orders of magnitude. While the median only shifts marginally, the width of the PDF increases, and with this the uncertainty of N_{INP} to a point where the right flank of the distribution (e.g. Fig. S1, black line) may only be interpreted as an upper limit.

It is worth mentioning, that due to the background subtraction, the PDFs may partly extend to nonphysical negative values. Altogether, interpreting results of a single sample that marginally exceeds the interference background is not ideal. However, multiple samples that are only slightly above the interference background may become distinguishable.

1.5 Merging of freezing spectra of LINA and INDA

This procedure of MC simulation and background subtraction was carried out for both results of LINA and INDA. LINA yields more accurate results at low temperature, while INDA is better suited for measurements at higher temperatures. In order to obtain continuous spectra covering a broad temperature range, results of both LINA and INDA were merged.

For low temperature (T < -21 °C) only LINA measurements were used as input, while at high temperatures (T > -17 °C) only INDA measurements are used. Between -17 °C and -21 °C, where both methods yield approximately equally accurate results and INP concentrations were averaged with equal weights, similar to Sze et al. (2023).

2 UTLS background INP dataset

2.1 Sample selection

To quantify UTLS background INP concentrations, ambient conditions during filter sampling are examined for UTLS background criteria. These criteria are: Firstly, the sample was collected exclusively above 4 km altitude, secondly the collected air mass was unaffected by recent deep convection and thirdly the air mass has not recently been transported upwards, e.g., within warm conveyor belts of low pressure systems. The check for convective influence was carried out manually by examining flight report, satellite data and trace gas measurements on board HALO (i.e. CO, CH4 and O3). The exclusion of air transported by warm conveyor belts was carried out via the aid of LAGRANTO backward trajectories calculated from the flight track (for more details see De La Torre Castro et al., 2023, where the same trajectory dataset was used). From a total of 28 aerosol samples obtained during CIRRUS-HL, 12 fulfill all criteria for the UTLS background.

These 12 samples were collected over a total time span of 33.1 hours, and accumulated a total sampling volume of 20.2 sm^{-3}. The sampling area is confined to the western, central and northern Europe UTLS (Fig. S3). The average sampling altitude is 10.6 km, the average ambient pressure 279 hPa and the average ambient temperature -41.7 °C (see Fig. S2 and Tab. S1 for more details on ambient sampling conditions). Notably, 95 % of the sampling was carried out in environments featuring temperatures below the homogeneous nucleation temperature of -37 °C (Fig. S2b). Regarding potential temperature and ozone concentration (Fig. S2a,d), the filters were collected in the lower stratosphere (roughly, Θ > 350 K, O_3 > 400 ppmv) and upper troposphere (roughly, Θ < 340 K, O_3 < 200 ppmv) to about equal proportions.

For further characterization of the UTLS background aerosol, analysis of single particle chemical composition is presented (Fig. 2). The ALABAMA instrument measured in parallel covering 89 % of the UTLS background filter sampling time. As shown in Fig. 2, the UTLS background aerosol is composed of a mix of typical lower stratospheric particles, i.e., meteoric material (Schneider et al., 2021; Murphy et al., 2014), and particles types commonly present in the upper troposphere, i.e., particles containing ammonium, sulfate, nitrate and/or organic compounds (Murphy et al., 2006).

The presence of biomass burning aerosol (BBA) in the upper troposphere in summer 2021 was widespread. In the lower stratosphere, BBA was mostly present in aerosol plumes. The source of BBA are likely Canadian wildfires, which were frequent and violent in summer 2021 (Parisien et al., 2023). Due to its omnipresence BBA and BBA plumes, BBA considered as part of the UTLS background here.

2.2 Merging freezing spectra into one dataset dataset

To simplify this dataset and to obtain a parameterization applicable in atmospheric models, the 12 UTLS background INP samples are merged by combining the subtracted MC INP spectra of the samples into one dataset. Taking into account the varying samples volumes (see Tab. S1), merging of the dataset was done via weighting the MC INP spectra of the UTLS samples depending on their sampling volume. Thus, the relative contribution to the dataset of a sample collected over a longer duration, with a larger sampling volume, is larger than those collected only over a short duration with a small sampling volume. The resulting combined dataset yield UTLS background INP PDF in 2 K temperature resolution (see Fig. S4a).

2.3 Exponential fit

The exponential fit was applied in accordance to Li et al. (2022), i.e., a weighted least squares fit of the medians within the temperature range, where the fraction of observations yielding $f_{ice} > 0$ and $f_{ice} < 1$ is larger than 50 %. The number of observations with frozen fraction $f_{ice} > 0$ and $f_{ice} < 1$ is used as weights. With this approach, values between -20 °C and -28°C have larger weights compared data points at > -20 °C, reducing systematic bias (Li et al., 2022). The obtained fit lies at the lower end or below typical mid-latitude INP concentrations (Petters and Wright, 2015) and aligns well with previous free tropsopheric background INP measurements at -30 °C (Lacher et al., 2018). To demonstrate the impact of interference background subtraction, uncorrected UTLS background INP concentration were fitted (Fig. S1, dashed blue line). The uncorrected fit yields values exceeding the subtracted fit by a factor between 1.4 to 2.1.

3 Droplet shattering at HASI

Aerosol sampling in liquid phase clouds using the HASI inlet can lead to droplet shattering artifacts, that likely occurred during the case study F15 in a short sampling section between 13:08 and 13:13. When cloud droplets collide with the inlet shroud or tip, they can shatter into numerous small droplets, which may deflect from the surface into the sampled airstream (Weber et al., 1998; Craig et al., 2013). Thereby, the amount of droplets entering the aerosol inlet is commonly higher than the ambient cloud droplet number concentration. These droplets are dried in the sampling line and the residues are detected as aerosol particles. Consequently, the measured concentration of aerosol particles is elevated.

The effect of droplet shattering on INP concentration in the sampling line has, to our knowledge, not been investigated. Because immersion freezing INPs are typically insoluble, only droplet shattering processes that increase the number of insoluble particles in the sampling line have the potential to also artificially increase the INP concentration in the sampling line. This would lead to an overestimation of INP concentration due to droplet shattering artifacts, but likely to a lesser degree than the overestimation of the aerosol particle concentration. Three different shattering scenarios can be regarded: Firstly, the shattering of droplets that contain only soluble non ice-active material, which would lead to an overestimation of the aerosol particle concentration in the sampling line but would not affect INP concentration. Secondly, the shattering of droplets containing insoluble ice-active aerosol particles, which could lead to an overestimation of both INP concentration and aerosol particle concentration if the shattered droplets are deflected from the surrounding air not sampled by the aerosol inlet into the sample airstream. And finally, the shattering of droplets containing insoluble aerosol particles that are originally already within the sampling air stream. This process would not alter INP concentration and aerosol concentration within the sampling line as the number of insoluble aerosol particles/INP does not increase when the droplets shatter.

With this, the uncertainty introduced by droplet shattering on INP is difficult to quantify. To mitigate this uncertainty to some degree, we normalize INP concentrations by the concentration of large aerosol particle n_{500} yielding activated INP fraction as aerosol particles generated by shattering are likely smaller than 500 nm Kleinman et al. (2012). This approach partially compensates for the uncertainty introduced by droplet shattering, making the activated INP fraction a robust metric in this study.

Table S1. list of samples adhering to UTLS background criteria, together with mean sampling altitude, mean ambient temperatures, and respective minima and maxima in brackets. Additionally, the sampling duration and sampling volume is given

flight	HERA Filter Position	date	h [km]	T [°C]	duration [min]	Volume (standard) [sm^{-3}]
F03	3	June 26	13.2 (10.1 / 14.2)	-48.6 (-56.5 / -44.5)	77	0.7
F05/06	2	June 29	11.0 (9.7 / 11.3)	-50.1 (-55.0 / -41.9)	105	1.3
F05/06	4	June 29	12.6 (8.0 / 14.1)	-47.7 (-60.6 / -32.1)	169	1.7
F08/09	2	July 05	13.0 (11.8 / 13.4)	-46.4 (-49.4 / -44.2)	141	1.3
F10/11	1	July 07	10.2 (6.1 / 12.6)	-44.2 (-54.5 / -16.0)	61	0.8
F10/11	3	July 07	13.5 (11.7 / 14.1)	-48.8 (-56.9 / -42.6)	326	2.8
F13/14	1	July 12	12.7 (4.1 / 14.0)	-44.4 (-58.1 / 0.4)	91	0.9
F18/19	1	July 19	13.2 (7.9 / 14.2)	-47.3 (-55.4 / -28.3)	238	2.2
F20/21	2	July 21	12.0 (6.0 / 13.7)	-49.5 (-60.1 / -7.5)	254	2.8
F22	3	July 23	12.5 (9.2 / 14.2)	-49.8 (-53.6 / -38.2)	214	2.2
F23	4	July 28	12.8 (6.6 / 14.1)	-45.4 (-55.3 / -17.1)	178	1.7
F24	5	July 29	10.0 (4.7 / 14.1)	-39.3 (-53.8 / -4.4)	133	1.8

Table S2. table of used abbreviations and acronyms

Deep Convective clouds	DCC
Ice-nucleating particle	INP
free troposphere	FT
CIRRUS in High Latitudes (HALO campaign name)	CIRRUS-HL
High and Long Range research aircraft (research aircraft)	HALO
Cloud particle residuals	CPR
High-volume flow aerosol particle filter sampler (instrument)	HERA
HALO counter flow virtual impactor	HALO-CVI
HALO sub-micrometer aerosol inlet	HASI
upper troposphere and lower stratosphere	UTLS
Biomass Burning Aerosol	BBA
Leipzig ice nucleation array	LINA
Ice nucleation droplet array	INDA
Aircraft-based laser ablation aerosol mass spectrometer	ALABAMA
Monte-Carlo	MC
probability density function	PDF

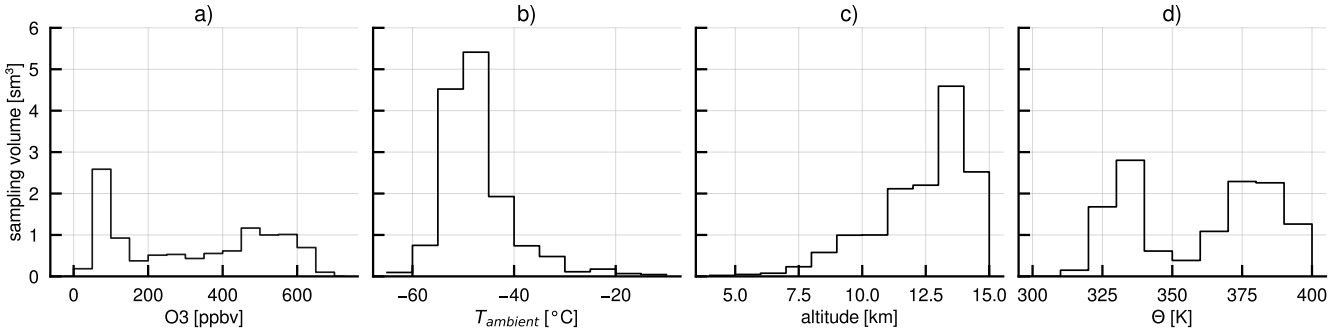

Figure S2. Distributions of the sampling volume for different environmental condition for the UTLS INP dataset. (a) shows sampling volume distributed by Ozone concentration, (b) by ambient temperature, (c) by altitude, and (d) by potential virtual temperature. The total sampling volume is $20.19\,\mathrm{sm}^3$.

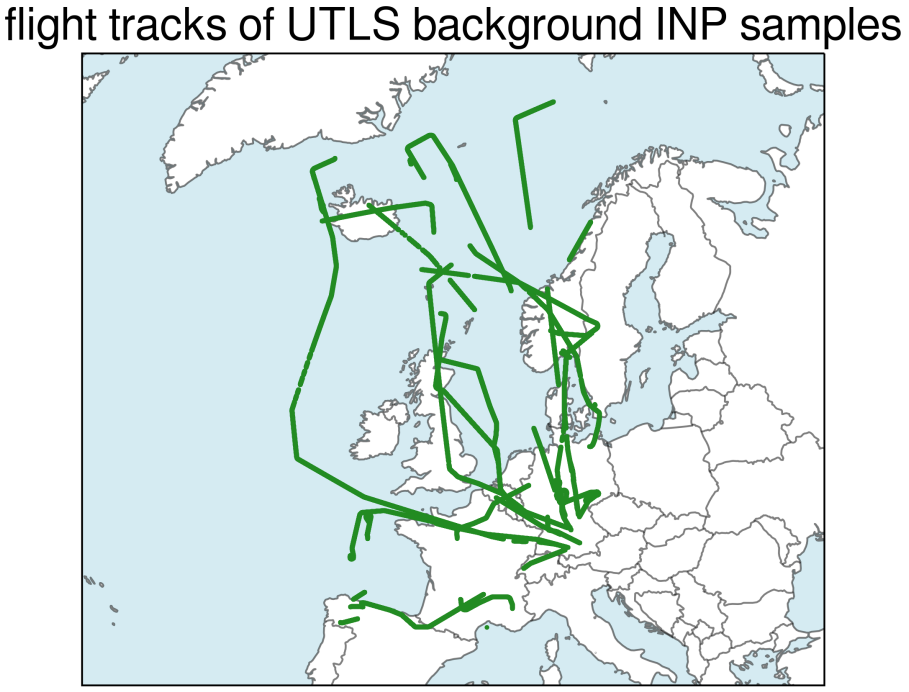

Figure S3. flight track/ sampling location of all UTLS background INP samples

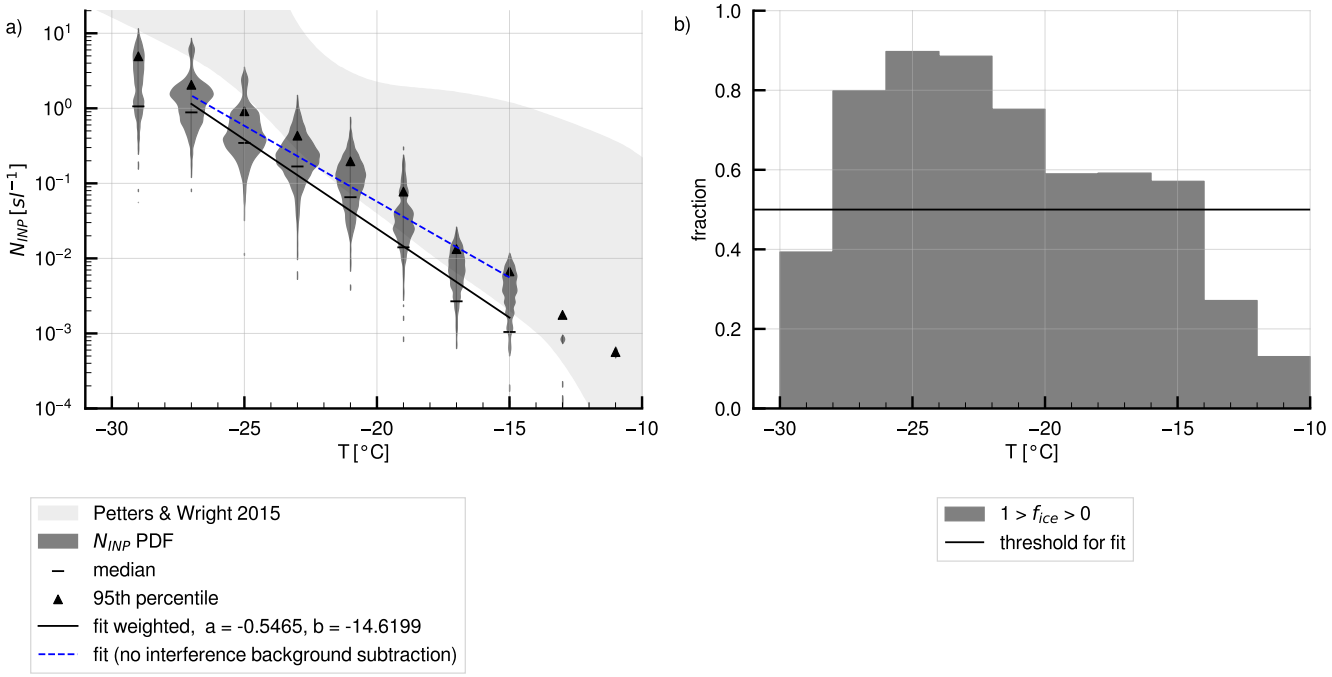

Figure S4. left panel (a): probability density functions of UTLS background INP concentrations at different effective temperatures. The interference background was subtracted and only positive values are shown together with an exponential fit (black line) $N_{\mathrm{INP}}(T) = exp(a \times T + b)$ with a = -0.5465, b = -14.6199. In contrast, the fit over the not subtracted dataset is shown by the dashed blue line. Medians of the PDFs are shown as horizontal line and the upper 95th percentile as triangle. In the background are typical mid-latitude INP concentrations derived from precipitation samples (Petters and Wright, 2015). right panel (b): fraction of interference background subtracted Monte-Carlo spectra with $0 < f_{\mathrm{ice}} < 1$. The frozen fraction $f_{\mathrm{ice}}$is the fraction of frozen droplets/wells in the offline INP analysis. Only temperature intervals with more than half of the observations yielding finite and non-zero N_{INP} (black threshold line) were used for the fit

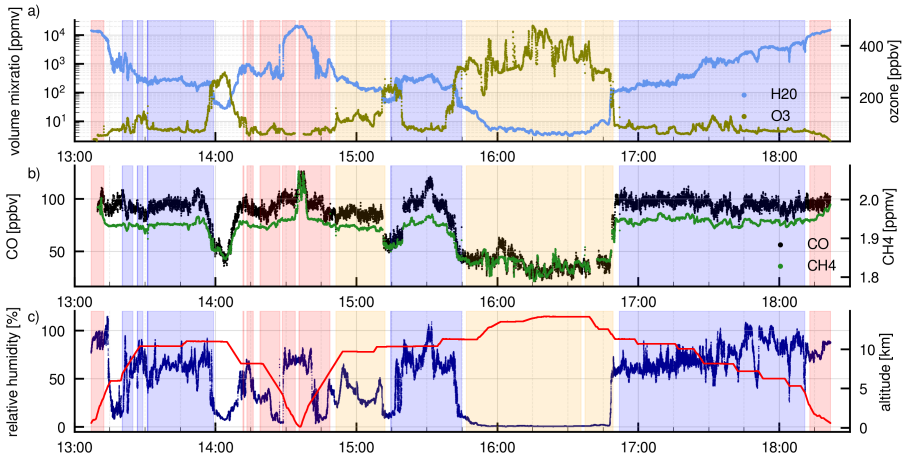

Figure S5. trace gas concentration throughout the case study of research flight 15 showing, water vapor (light blue), ozone (olive), carbon monoxide (black), methane concentrations (green), relative humidity with respect to water (dark blue) and flight altitude (red). The instrument setup is described in Jurkat-Witschas et al. (2025). The underlying colors again mark HERA filter sampling times section identical to Fig.3 (main text)

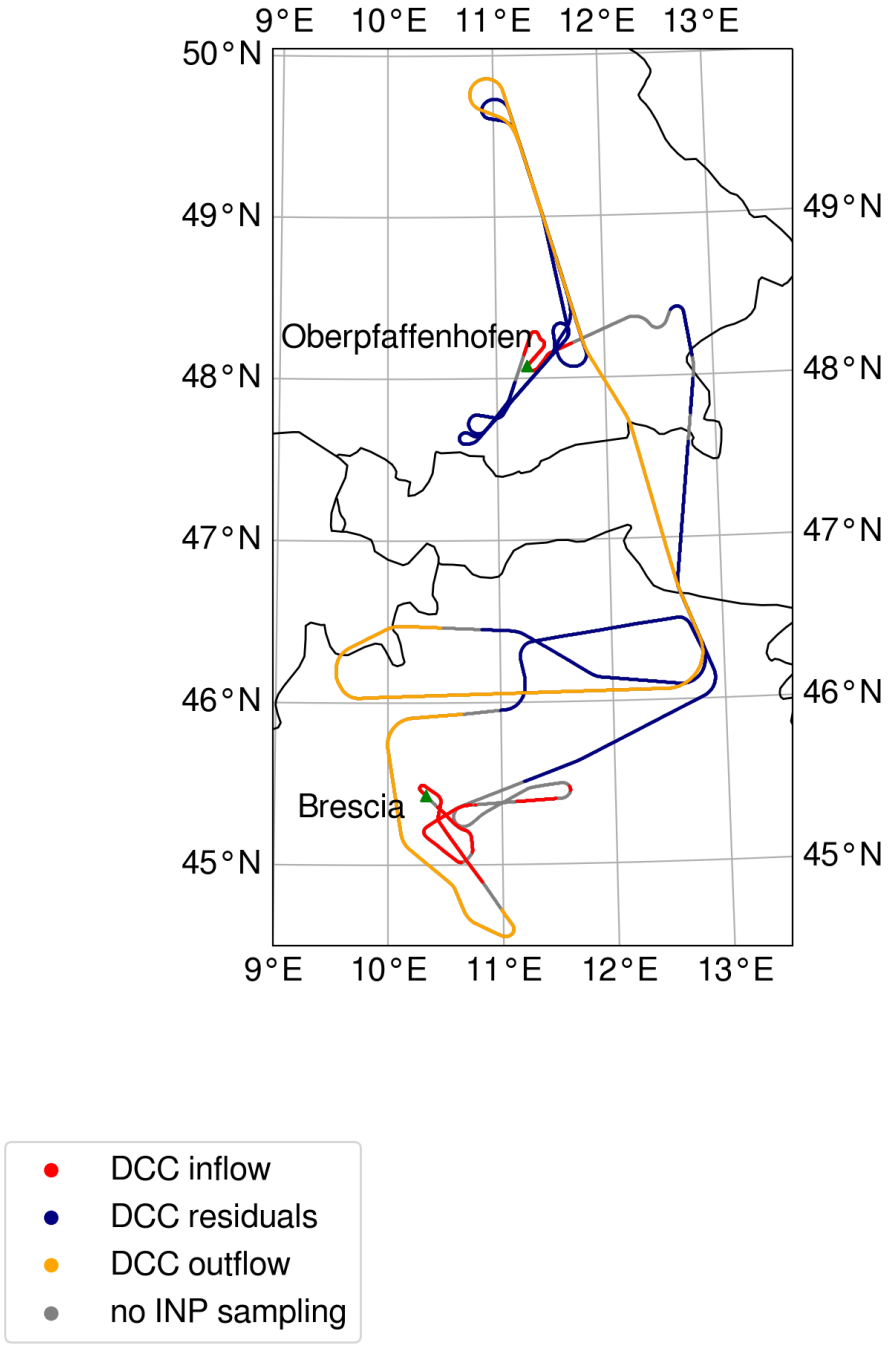

Figure S6. same as Fig. 2 but only showing the flight track of F15 and marked sampling sections.

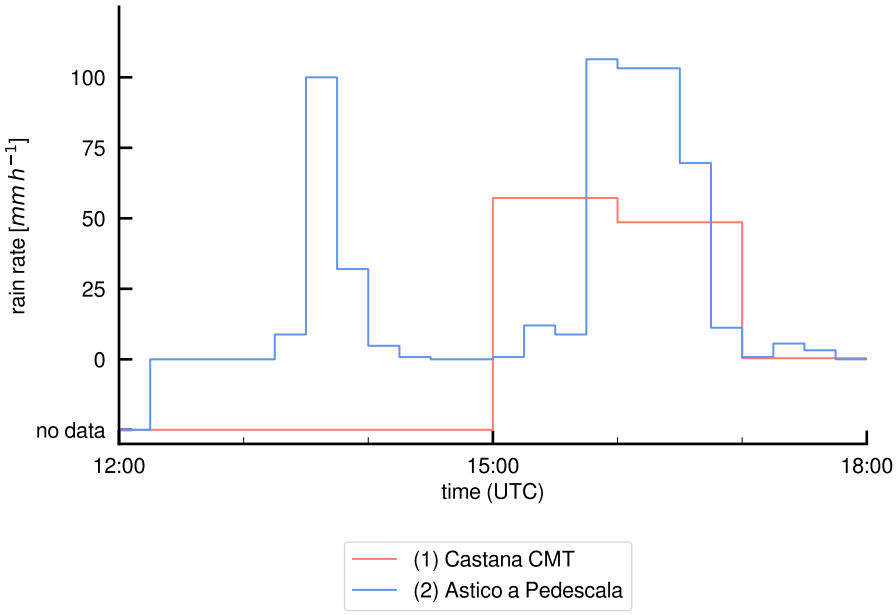

Figure S7. ground measurements of precipitation by two automatic weather stations in the Veneto region. Both weather station were situated right beneath the DCC shown in Fig. 2. Note that Castana CMT precipitation data is hourly, while Astico a Pedescale is obtained in 15 min intervals. The weather stations are operated by the Italian Civil Protection Department Veneto and the date is available at the open data platform Mistral Meteo-Hub (Bottazzi et al., 2021)

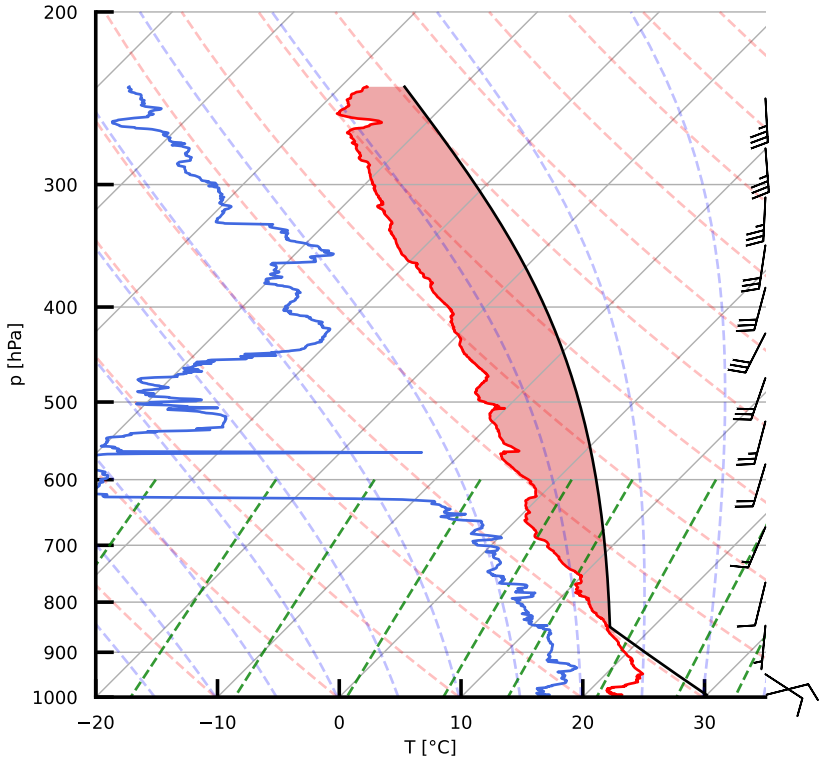

Figure S8. vertical temperature (red line) and dew point (blue line) profile measured by HALO during the descent to Brescia Airport from 14:15 to 14:30 UTC shown in a skew-T diagram. Wind bards indicate wind speed and direction. At the time of the dive the area was mostly cloud free but the profile shows in which environment and air mass the DCC are formed. To get an estimate for the lifting profile of the DCC shown in Fig. 2, ground observation of the Verona-Villafranca weather station at 16 UTC were used. These indicate with T = 30 °C and dew point τ = 19 °C, and consequently a lifting condensation level at 848 hPa and 16.5 °C as an estimate for the cloud base temperature. The convective available potential energy (CAPE) above that lifting condensation level would be 2489 J kg^{-1}

References

Bottazzi, M., Scipione, G., Marras, G. F., Trotta, G., D'Antonio, M., Chiavarini, B., Caroli, C., Montanari, M., Bassini, S., Gascón, E., et al.: The Italian open data meteorological portal: MISTRAL, Meteorological Applications, 28, e2004, 2021.

Craig, L., Moharreri, A., Schanot, A., Rogers, D. C., Anderson, B., and Dhaniyala, S.: Characterizations of cloud droplet shatter artifacts in two airborne aerosol inlets, Aerosol Science and Technology, 47, 662–671, 2013.

De La Torre Castro, E., Jurkat-Witschas, T., Afchine, A., Grewe, V., Hahn, V., Kirschler, S., Krämer, M., Lucke, J., Spelten, N., Wernli, H., Zöger, M., and Voigt, C.: Differences in microphysical properties of cirrus at high and mid-latitudes, Atmospheric Chemistry and Physics, 23, 13 167–13 189, https://doi.org/10.5194/acp-23-13167-2023, 2023.

Harris, C. R., Millman, K. J., van der Walt, S. J., Gommers, R., Virtanen, P., Cournapeau, D., Wieser, E., Taylor, J., Berg, S., Smith, N. J., Kern, R., Picus, M., Hoyer, S., van Kerkwijk, M. H., Brett, M., Haldane, A., del Río, J. F., Wiebe, M., Peterson, P., Gérard-Marchant, P., Sheppard, K., Reddy, T., Weckesser, W., Abbasi, H., Gohlke, C., and Oliphant, T. E.: Array programming with NumPy, Nature, 585, 357–362, https://doi.org/10.1038/s41586-020-2649-2, 2020.

Jurkat-Witschas, T., Voigt, C., Groß, S., Kaufmann, S., Sauer, D., De la Torre Castro, E., Krämer, M., Schäfler, A., Afchine, A., Attinger, R., et al.: CIRRUS-HL: Picturing High-and Midlatitude Summer Cirrus and Contrail Cirrus above Europe with Airborne Measurements aboard the Research Aircraft HALO, Bulletin of the American Meteorological Society, 106, E2300–E2327, 2025.

Kleinman, L. I., Daum, P. H., Lee, Y.-N., Lewis, E. R., Sedlacek Iii, A., Senum, G., Springston, S., Wang, J., Hubbe, J., Jayne, J., et al.: Aerosol concentration and size distribution measured below, in, and above cloud from the DOE G-1 during VOCALS-REx, Atmospheric Chemistry and Physics, 12, 207–223, 2012.

Lacher, L., DeMott, P. J., Levin, E. J., Suski, K. J., Boose, Y., Zipori, A., Herrmann, E., Bukowiecki, N., Steinbacher, M., Gute, E., et al.: Background free-tropospheric ice nucleating particle concentrations at mixed-phase cloud conditions, Journal of Geophysical Research: Atmospheres, 123, 10–506, 2018.

Li, G., Wieder, J., Pasquier, J. T., Henneberger, J., and Kanji, Z. A.: Predicting atmospheric background number concentration of ice-nucleating particles in the Arctic, Atmospheric Chemistry and Physics, 22, 14 441–14 454, 2022.

Murphy, D., Cziczo, D., Froyd, K., Hudson, P., Matthew, B., Middlebrook, A., Peltier, R., Sullivan, A., Thomson, D., and Weber, R.: Single-particle mass spectrometry of tropospheric aerosol particles, Journal of Geophysical Research: Atmospheres, 111, 2006.

Murphy, D., Froyd, K., Schwarz, J., and Wilson, J.: Observations of the chemical composition of stratospheric aerosol particles, Quarterly Journal of the Royal Meteorological Society, 140, 1269–1278, 2014.

Parisien, M.-A., Barber, Q. E., Bourbonnais, M. L., Daniels, L. D., Flannigan, M. D., Gray, R. W., Hoffman, K. M., Jain, P., Stephens, S. L., Taylor, S. W., et al.: Abrupt, climate-induced increase in wildfires in British Columbia since the mid-2000s, Communications Earth & Environment, 4, 309, 2023.

Petters, M. and Wright, T.: Revisiting ice nucleation from precipitation samples, Geophysical Research Letters, 42, 8758–8766, 2015.

Schneider, J., Weigel, R., Klimach, T., Dragoneas, A., Appel, O., Hünig, A., Molleker, S., Köllner, F., Clemen, H.-C., Eppers, O., et al.: Aircraft-based observation of meteoric material in lower-stratospheric aerosol particles between 15 and 68° N, Atmospheric chemistry and physics, 21, 989–1013, 2021.

Sze, K. C., Wex, H., Hartmann, M., Skov, H., Massling, A., Villanueva, D., and Stratmann, F.: Ice-nucleating particles in northern Greenland: annual cycles, biological contribution and parameterizations, Atmospheric Chemistry and Physics, 23, 4741–4761, 2023.

Vali, G.: Quantitative evaluation of experimental results an the heterogeneous freezing nucleation of supercooled liquids, Journal of Atmospheric Sciences, 28, 402–409, 1971.

Vali, G.: Revisiting the differential freezing nucleus spectra derived from drop-freezing experiments: methods of calculation, applications, and confidence limits, Atmospheric Measurement Techniques, 12, 1219–1231, 2019.

Weber, R., Clarke, A., Litchy, M., Li, J., Kok, G., Schillawski, R., and McMurry, P.: Spurious aerosol measurements when sampling from aircraft in the vicinity of clouds, Journal of Geophysical Research: Atmospheres, 103, 28 337–28 346, 1998.